High temperature chromium volatilization from Cr2O3 powder and Cr2O3-doped UO2 pellets in reducing atmospheres

Véronique Peres, Loïc Favergeon, Marie Andrieu, Jean-Claude Palussière, Julien Balland, Christine Delafoy, Michèle Pijolat

Journal of Nuclear Materials, 2012, 423(1-2), 93-101, doi: 10.1016/j.jnucmat.2012.01.001

High temperature chromium volatilization from Cr_2O_3 powder and Cr_2O_3-doped UO_2 pellets in reducing atmospheres

VÉRONIQUE PERES[1]*, LOÏC FAVERGEON[1], MARIE ANDRIEU[1,2], JEAN-CLAUDE PALUSSIÈRE[2], JULIEN BALLAND[2], CHRISTINE DELAFOY[3], MICHÈLE PIJOLAT[1]

[1] *Ecole Nationale Supérieure des Mines de Saint Etienne, Centre SPIN ; Département PRESSIC ; LPMG -UMR CNRS 5148, 158 Cours Fauriel - 42023 Saint-Étienne Cedex 2, France*
[2] *Areva NP, FBFC, Avenue de la déportation 26104 Romans/Isère, France*
[3] *Areva NP, 10 rue Juliette Récamier, 69456 Lyon, France*

Abstract

Chromium volatilization from Cr_2O_3 powder and Cr_2O_3-doped UO_2 pellets during sintering in reducing atmospheres has been studied by thermogravimetry (TG) coupled with differential thermal analysis (DTA) up to 1700°C. The sintering of Cr_2O_3-doped UO_2 pellets was also followed by dilatometry. Oxygen partial pressures in the range 10^{-20}-10^{-11} atm (10^{-15}-10^{-6} Pa) have been fixed in all the experiments thanks to mixtures of hydrogen and carbon dioxide. A linear heating rate of 20°C min^{-1} was applied to all the experiments. The dopant amount was in the range 0.18-0.9 mol% Cr in UO_2. For all the oxygen potentials, the mass loss of Cr_2O_3 powder was found to start at temperatures as high as 1470°C due to Cr_2O_3 dissociation, the lower the oxygen potential, the lower the starting temperature and the higher the volatilized amount. For intermediate oxygen potentials, an exothermic DTA peak observed during cooling, from 1700°C to room temperature, attested for the crystallization of a liquid phase which was attributed to $CrO_{(l)}$ according to thermodynamic predictions. Then, the dilatometry and TG studies allowed following the behavior of Cr_2O_3-doped UO_2 pellets. The mass loss at temperatures higher than 1470°C was attributed to chromium volatilization for all the doped samples. During the sintering of doped UO_2 pellets, the liquid phase $CrO_{(l)}$ seemed to appear at a lower oxygen potential than in Cr_2O_3 powder, which probably contributed to enhance the densification rate. For the highest dopant amount, 0.9 mol% Cr, the volatilization process was found to be rather similar to that of Cr_2O_3 powder, due to the part of chromia not solubilized in the UO_2 crystal. Moreover, as the initial pellets were not dense, as long as the pellet porosity remained open, the chromia particles were able to dissociate as in the Cr_2O_3 powder. Thus the volatilization of chromium from doped UO_2 pellets under sintering in reducing atmospheres must be understood as the result of several phenomena whose contribution depends on temperature, oxygen potential and heating rate: before the porosity closure, both dissociation of chromia into $Cr_{(g)}$ and oxygen from excess Cr_2O_3 particles, and Cr volatilization from doped UO_2 particles; then chromium volatilization from the doped UO_2 ceramic during further densification process.

* Corresponding author : peres@emse.fr

Journal of Nuclear Materials, 2012, 423(1-2), 93-101, doi: 10.1016/j.jnucmat.2012.01.001

Keywords:
Chromium volatilization ; Cr_2O_3 powder ; Cr_2O_3-doped UO_2 pellets ; sintering ; reducing atmospheres

I. Introduction

Upgrading the economics of light-water reactor plants leads to increased demands on reactor maneuverability with continued enhancement of fuel performance and reliability. Research on fuel pellets focuses on the ability of large grain and visco-plastic UO_2 microstructure to increase fission products retention and pellet mechanical compliance [1]. High expectations are placed on the optimized chromia-doped UO_2 fuel developed by Areva NP which exhibits significantly higher performance compared to the reference UO_2 fuel [2]. In the first development step started in the 1990's, the fundamental mechanisms governing UO_2 doping with Cr_2O_3 were clarified. The sintering conditions have been optimized to enhance chromia dissolution in the UO_2 matrix and to increase the solubility limit of chromium into UO_2 [3] and [4]. To master the doped UO_2 fuel fabrication technology, a large industrialization program has been launched to study the evolution of the pellet characteristics as a function of various parameters: U_3O_8 recycling, pellet sintering conditions, etc. Optimized manufacturing conditions are now defined to ensure the reproducibility of the targeted microstructure changes with a reduced scattering inside a pellet lot or between lots.

In parallel, fundamental researches are in progress such as the present study which aims to understand in depth the behavior of Cr_2O_3 at high temperature. Toker *et al.* [5] studied the thermodynamic properties and phase relations of the Cr-O system at temperatures from 1500 up to 1825°C. The outcome thermodynamic diagram, shown in Figure 1, defines domains of existence for several phases $Cr_{(s)}$, $Cr_2O_{3(s)}$, $Cr_3O_{4(s)}$ and $CrO_{(l)}$ versus temperature and oxygen potential (oxygen partial pressures in the range of 10^{-20} - 10^{-11} atm/10^{-15} - 10^{-6} Pa). Johnson and Muan [6] also studied a binary phase diagram from mixtures of Cr_2O_3 and Cr powders in a purified argon atmosphere and showed the existence of an eutectic at 1665°C. This value is closed to the one found previously by Ol'Shanskii and Shlepov [7] who reported an eutectic temperature at 1660°C. In such high temperature and low oxygen pressure conditions, chromium is suspected to "evaporate" from the solid phase; however at our knowledge, neither mechanism nor quantitative data on this phenomenon in reduced atmospheres are available. This article presents first a thermogravimetry study coupled with differential thermal analysis (TG-DTA) of a chromia powder in the range of temperatures 1100-1700°C in reducing atmospheres (oxygen pressure in the range of 10^{-20} - 5 x 10^{-11} atm/10^{-15} - 10^{-6} Pa). Then the behavior of chromia-doped UO_2 pellets followed by TG and dilatometry in the same thermodynamic conditions is discussed with the help of the results obtained with the Cr_2O_3 powder.

II. Experimental

II.1. Materials

The Cr_2O_3 powder (Elementis) used in this study, has a purity grade of 99.794%, the main impurities are calcium (410 ppm) and silicium (1100 ppm). Its specific surface area has been determined by the BET method with the Kr adsorption isotherm at a temperature of 75 K. A value of 6.0 $m^2\ g^{-1}$ was found, to which corresponds an average diameter of 0.19µm for primary particles according to the assumption that Cr_2O_3 particles are spherical.
The chromia-doped UO_2 pellets (noted Cr-doped UO_2 in the following) used for the TG analyses are small disks with a reduced thickness of ~2 mm and a diameter of ~9 mm. Such geometry is required to avoid edge effects and consider a planar symmetry. The samples have been prepared by Areva NP (manufacturing plant of FBFC Dessel, Belgium) from depleted UO_2 powder converted by the dry route process and without any other additives. This UO_2 powder is slightly overstoichiometric ($UO_{2.069}$) and its purity grade is 99.9954%. The specific surface area of this powder is equal to 2.4 $m^2\ g^{-1}$ with an equivalent particle diameter of 0.23µm. The chromia powder is directly added to UO_2 at the blending step. After pre-compaction and granulation operations, the pellets have been compacted to a green density level of ~6 g cm^{-3}.

The doped UO_2 samples studied by dilatometry were manufactured according to the same process and same materials.
However, sample pellets with a cylinder form (~7 mm thickness and ~10 mm diameter) were required to obtain a measurable signal during densification. For the present work, several Cr_2O_3 contents have been studied: undoped UO_2, UO_2 + 0.18 mol% Cr (589 ppm Cr_2O_3), UO_2 + 0.44 mol% Cr (1419 ppm Cr_2O_3) and UO_2 + 0.9 mol% Cr (2878 ppm Cr_2O_3).

II.2. Experimental methods

II.2.1. TG and DTA experiments

The thermogravimetry (TG) experiments have been performed with a symmetrical balance (SETARAM TAG 24) equipped with a differential thermal analysis (DTA) device (tungsten crucibles and W-5%Re/W-26%Re thermocouples) appropriated to high temperature conditions (maximum 1700°C) and to reducing atmospheres. The device is connected to a gas panel equipped with H_2 and CO_2 mass flowmeters to fix the desired amount of CO_2 in hydrogen: 0.6% CO_2, 1.11% CO_2, 1.47% CO_2, 2.06% CO_2 and 3.2% CO_2. Before introduction of the gas mixture, the device is evacuated to 10^{-4} atm (10 Pa) to eliminate residual gases. The CO_2 content in the exit gas was ascertained by infrared spectrometry at room temperature. The measured error was ±0.02% CO_2 in the mixture. The oxygen potentials equivalent to the H_2/CO_2 mixtures were obtained according to Deines *et al.*'s data [8]; they have been reported as a function of temperature in Figure 1a; it can be seen that the lines corresponding to the experimental conditions cross interesting domains of the thermodynamic diagram. The estimated error on the oxygen potential, based on the CO_2 content measurement, corresponds to ±250 J mol^{-1}. The experiments have been conducted up to 1700°C with a heating rate of 20°C min^{-1} followed by a soaking time of five minutes to compensate the thermal inertia of the furnaces and a cooling rate of 30°C min^{-1}. As a consequence, the very last part of the DTG and DTA curves will not be commented.
To reach uniform thermal and gaseous composition conditions within the powdered samples, the TG-DTA experiments were achieved with ~3 mg of Cr_2O_3 which corresponds to a powder bed as thin as of ~0.5 mm in the crucible. TG-DTA blank tests were performed without any sample in the crucible to monitor the baseline of the mass and DTA signals. The mass signal exhibited a continuous drift which did not exceed 35µg from 1400°C to 1700°C. The mass loss curves were corrected by subtraction of this baseline. The reproducibility of the mass loss curves versus temperature was good: ±0.3 wt%. Concerning the DTA curves, the onset and maximum peak temperatures were reproducible with an accuracy of ±1.5°C. However some problems of reproducibility were encountered in the case of DTA since for two identical experiments, the shape of the signals was not rigorously reproducible, probably due to the small amount of sample in the crucible. To follow the chromium volatilization from Cr-doped UO_2 pellets, TG experiments were done placing a pellet of ~0.8 g in a tungsten crucible suspended to a tungsten suspension (it was not possible to use the TG-DTA device due to the limited amount of sample in the DTA crucible).

II.2.2. Dilatometry tests

All the dilatometry tests were performed at the Areva NP Ceramic Laboratory in Erlangen (Germany) by means of a Netzch device (DIL 402 C) allowing to work up to 2000°C under H_2/CO_2 mixtures. The shrinkage measurement resolution, gave by the provider, is 0.125 nm/1.25 nm but the operational shrinkage precision was not better than 1µm. The tests were conducted up to 1700°C in the same atmospheres than those used in the thermobalance, with a heating and a cooling rate of 20°C min^{-1}. The results were analyzed by reference to the theoretical density which is 10.96 g cm^{-3} for UO_2, and respectively 10.95, 10.94 and 10.93 for the 0.18%, 0.44% and 0.9 mol% Cr doped samples.

III. Results and discussion

III.1. TGA–DTA study of Cr_2O_3 powder

Figures 2(a-e) shows the experimental curves of mass loss (TG), derivative of mass loss (DTG) and heat flow (DTA) obtained for the Cr_2O_3 powder under the various H_2/CO_2 atmospheres. Neither mass loss nor DTA signals were observed below 1400 °C, so the results are presented between 1400 °C and 1700 °C. The mass loss due to the chromium volatilization was observed to begin in the temperature range 1430-1660 °C, depending on the oxygen potential, the higher the oxygen potential, the higher the onset temperature. All the experiments except for the highest oxygen potentials (3.2% CO_2) exhibited an endothermic signal during the heating treatment. An exothermic signal was observed during cooling for the experiments done with 1.47% CO_2 and 2.06% CO_2 mixtures (*cf.* Figures 2c and d). The results of the TG and DTA tests (onset and peak temperatures, final mass loss) are summarized in Table 1. The onset temperature for TG and DTA signals during heating are quite similar for 0.6% and 1.11% CO_2, whereas the DTA endothermic peak starts before the TG mass loss for 1.47% and 2.06% CO_2. It can be noticed that the higher the oxygen potential, the lower the total mass loss (*cf.* 4th line of Table 1). In order to explain the TG-DTA results, we have listed in Table 2 the most probable reactions that could occur considering the various condensed phases appearing in the thermodynamic diagram ($Cr_2O_{3(s)}$, $Cr_{(s)}$, $Cr_3O_{4(s)}$ and $CrO_{(l)}$):

- dissociation of Cr_2O_3 into gaseous or solid metallic chromium and oxygen (reactions R1 or R2, respectively),
- chromium evaporation from solid metallic chromium (reaction R3)
- decomposition of Cr_2O_3 into Cr_3O_4 (reaction R4),
- decomposition of Cr_3O_4 into gaseous or solid metallic chromium and oxygen (reactions R5 or R6, respectively),
- decomposition of Cr_3O_4 into liquid CrO and oxygen (reaction R7),
- decomposition of $CrO_{(l)}$ into gaseous chromium and oxygen (reaction R8),
- decomposition of Cr_2O_3 into $CrO_{(l)}$ and oxygen (reaction R9),
- vaporization of $CrO_{(l)}$ into gaseous CrO (R10),
- reaction of $Cr_{(g)}$ with $Cr_2O_{3(s)}$ to form liquid CrO (R11).

For each reaction the values of the corresponding standard enthalpy variations and Gibbs energy variations calculated at 1400°C and 1700°C [9] and [10] have been reported in Table 2 as well as the theoretical mass losses at total conversion. In Figure 1a have been reported the temperatures observed for the DTA peak onsets during heating (dots) and the mass loss onsets (triangles). It can be seen that for all atmospheres, the mass loss and the endothermic effect begins well before the limits of the phase diagram. This means the volatilization process begins to be detected without appearance of a new solid or liquid phase. Moreover, the onset temperature increases when the oxygen potential increases.

Figure 3 represents the equilibrium pressures of the gaseous species $Cr_{(g)}$, $CrO_{(g)}$, $CrO_{2(g)}$, $CrO_{3(g)}$ as a function of temperature, calculated considering the change in oxygen potential with temperature in the atmosphere 1.11% CO_2 (*cf.* line 2 in Figure 1a) and for the various condensed phases of Toker's diagram. It can be seen that gaseous chromium is the most probable species that can be released whatever the condensed phase would be; considering the other atmospheres, the calculations (results not shown) lead to the same observation. Moreover Figure 4, which represents for reaction R1 the gaseous chromium equilibrium pressure *vs.* temperature for the various atmospheres, indicates that the higher the content in CO_2, the lower the $Cr_{(g)}$ partial pressure. It can thus be inferred from these thermodynamic considerations that the beginning of TG and DTA curves of Figure 2 corresponds to the dissociation of chromia according to reaction R1, in agreement with a high standard enthalpy value (1891 kJ mol^{-1} at 1400°C). When the temperature increases, the equilibrium pressure in

$Cr_{(g)}$ increases, and so does the mass loss. The Cr_2O_3 dissociation process will continue provided the surface of the chromia particles remains in contact with the gas phase.
In the case of the most reducing atmosphere (0.6% CO_2), the thermodynamic diagram predicts that chromia would start to dissociate into solid metallic chromium $Cr_{(s)}$ and oxygen according to reaction R2 at 1470°C; since the final mass loss was found to exceed 31%, such a transformation must take place in parallel with R1 until chromia particles become totally covered with metallic chromium. Obviously mass loss due to reaction R3 has to be considered as soon as $Cr_{(s)}$ appear at the surface of the oxide particles (*cf.* Figure 2a). The large difference between the enthalpies of reactions R2 and R3 probably explains the difference in the peak temperatures of both DTG and DTA signals.
For the 1.11% CO_2 atmosphere, in addition to reaction R1 which is detected from 1499°C from TG and 1487°C from DTA (*cf.* Figure 2a), the formation of $Cr_3O_{4(s)}$ phase is expected at a temperature around 1650°C according to Toker *et al.* thermodynamic diagram. Above 1650°C four different reactions can occur: the formation of $Cr_3O_{4(s)}$ (R4), the dissociation of $Cr_3O_{4(s)}$ in gaseous chromium (R5), the dissociation of $Cr_3O_{4(s)}$ in solid chromium (R6) and the vaporization of solid chromium (R3). Reactions R4 and R5 could start at 1650°C against 1665°C for reactions R3 and R6. In this temperature range, the corresponding mass losses should be low because during the experiment, the $Cr_3O_{4(s)}$ domain is crossed during 10-20 s only, due to the high heating rate (20°C min^{-1}). In consequence the formation of $Cr_3O_{4(s)}$ should be rather limited; that could explain why the shape of the DTA and mass losses signals observed in Figure 2b are very similar to those of Figure 2a. When the temperature reaches 1665°C, reaction R2 may occur and subsequently reaction R3, both responsible for the mass loss. The final mass loss is lower than in the most reducing atmosphere since the reactions R2 and R3 are shifted at higher temperatures and the $Cr_{(g)}$ equilibrium pressure is lower.
With the 1.47% CO_2 atmosphere (*cf.* Figure 2c), similarly to the previous atmospheres, the phenomenon observed to begin at 1526°C for the mass loss and at 1470°C for the endothermic DTA signal should correspond to the reaction R1. Then, according to the thermodynamic diagram, two new phases can be considered: $Cr_3O_{4(s)}$ that can be formed by reaction R4 (chromia decomposition) and $CrO_{(l)}$, that can be formed by reactions R7 (Cr_3O_4 decomposition) and R9 (Cr_2O_3 decomposition). These three reactions might all contribute to the mass loss and DTA signals, and in addition, the dissociation (R8) of the liquid phase $CrO_{(l)}$ and its vaporization (R10) may also be involved. However, no particular feature could be noticed on the curves of Figure 2c. Thus as previously proposed, the period in the Cr_3O_4 domain is too brief to consider a significant contribution of reaction R4 to the mass loss. During the cooling, an exothermic peak without mass change has been identified which starts at 1663°C. This indicates a crystallization phenomenon from a liquid phase, *i.e.* the presence of $CrO_{(l)}$ seems to be confirmed. Due to their low standard enthalpies, reactions R7 and R9 (*cf.* Table 2) do not produce any characteristic peak on the endothermic DTA signal during heating.
In the 2.06% CO_2 atmosphere, according to Figure 1, only the dissociation of Cr_2O_3 can be envisaged. However, an exothermic signal has been observed during the cooling, at 1662°C, indicating again the crystallization from a liquid phase. This means that $CrO_{(l)}$ can be produced at lower temperature than predicted by the thermodynamic diagram (Figure 1) since according to Toker's data the $CrO_{(l)}$ phase should form at 1716°C. First, experimental errors on temperature or oxygen potential values have been considered to explain such difference from thermodynamic prediction. Considering the tungsten thermocouple precision (1.5°C), a temperature error can be excluded. As illustrated by Figure 1b, the error on the oxygen potential cannot explain the difference between the experimental oxygen potential and the $Cr_2O_{3(s)}/CrO_{(l)}$ equilibrium value at 1700°C. Another possible explanation could be the effect of impurities, as reported by Li *et al.* [11] who studied the sintering behavior of Cr_2O_3 in presence of ZrO_2. The thermodynamic diagram for the Cr-O system calculated for a $CrO_{(l)}$ activity of 0.8 reveals a larger domain of existence of $CrO_{(l)}$ than that proposed by Toker. So since the chromia powder contains silicium and calcium, their effect on the temperature of appearance of $CrO_{(l)}$ cannot be excluded.
In the case of the less reducing atmosphere 3.2% CO_2, the mass loss has been observed to start at 1659°C and there is no visible DTA signal. The mass loss seems to correspond to the

dissociation of Cr_2O_3 (reaction R1), the equilibrium metallic chromium partial pressure being 5.41 x 10^{-5} atm at 1659°C. The mass loss is very low even at 1700°C, which is in agreement with a lower equilibrium partial pressure for higher oxygen potentials, as previously discussed and illustrated by Figure 4. For this atmosphere, the conditions at 1700°C are quite far from the thermodynamic predictions for the $CrO_{(l)}$ domain (1750°C), which is consistent with the absence of a DTA exothermic signal during the cooling, probably due to an insufficient impurities effect.

III.2. Cr-doped UO_2 pellets

III.2.1. Dilatometry results

Table 3 reports some characteristic temperatures and density values obtained in all the dilatometry experiments with the undoped and 0.18%, 0.44% and 0.9% mol Cr-doped UO_2 pellets. Figure 5a represents the dilatometry curves *vs.* temperature for a sintering cycle in 2.06% CO_2 atmosphere, and the corresponding derivative curves showing the rate of densification are shown in Figure 5b. All the doped samples show a delay in the densification compared to UO_2. It is worthwhile to notice for doped samples the presence of a slight acceleration of the densification rate at temperatures around 1250°C. The temperature of the corresponding maximum has been reported in the 4th line of Table 3. This phenomenon, which is absent of the curves with the undoped UO_2, will be discussed in the next sections. The effect of the dopant on the final density, reported in the 6th line of Table 3, appears to depend both on the amount of dopant and on the atmosphere composition. The temperature corresponding to 94-95% of theoretical density was seen to depend on the gaseous atmosphere, as illustrated by Figure 6 which represents the derivative of the density *vs.* density obtained with undoped and 0.9 mol% Cr-doped UO_2 for 0.6%, 1.47%, 2.06% and 3.2% of CO_2. On each graph of Figure 6, the vertical line corresponds to 95% of the theoretical density, which is considered as the theoretical limit of existence of open pores in ceramics; beyond that value, it can be considered that there is no longer open porosity in the pellets. For 0.6% CO_2 the porosity remains open even at 1700°C whereas for 1.47%, 2.06% and 3.2% CO_2 the closure of the porosity is found near 1700°C. A maximum in the densification rate appears in the case of the doped samples near 1660°C for 1.47% CO_2 and 2.06% CO_2 and near 1680°C for 3.2% CO_2. These temperatures correspond rather well to those of the porosity closure. This will be discussed later in Section III.3.

III.2.2. TG analysis at H_2 + 1.47% CO_2

The curves of mass loss from room temperature to 1700°C in the 1.47% CO_2 atmosphere are shown in Figure 7a for 0.9 mol% Cr-doped and undoped samples. Figure 7b represents the rate of mass loss deduced from the curves of Figure 7a. During the heating up to around 1400°C, after a first mass loss (peak at 155°C and 270°C) due to water desorption, a second mass loss (peak at 420-440°C) is observed as the result of the UO_{2+x} reduction. The reduction process is achieved at about 1480°C for both samples. This can easier be observed on the curves of Figure 8 which represents an enlargement of the TG and DTG signals in the region 800-1700°C for undoped and doped samples (0.18, 0.44 and 0.9 mol% Cr) in 1.47% CO_2 atmosphere. In addition, in the DTG curves of Figure 8b, it appears a small shoulder close to 1200°C on the high temperature side of the large peak of the end of the UO_{2+x} reduction. Such a feature must be compared to the acceleration in the densification previously mentioned in Section III.2.1. A significant increase in the mass loss rate of the doped sample begins when the temperature exceeds 1480°C. This temperature is nearly the same as that observed for the beginning of chromia volatilization in the TG/DTA experiments of Cr_2O_3 powder sample at 1.47% CO_2. By analogy to the chromia powder results, this phenomenon thus can be mainly attributed to the dissociation of chromium oxide Cr_2O_3 (reaction R1).

III.3. Discussion

III.3.1. Volatilization from Cr_2O_3 powder

The TG–DTA experiments with chromia powder have shown that chromia may dissociate releasing metallic gaseous Cr (and oxygen) as the major volatile species whatever the atmosphere composition and the temperature could be. According to the oxygen potential and the temperature, other reactions should contribute to the volatilization process, as for example the vaporization of solid metallic chromium or liquid $CrO_{(l)}$. The presence of $CrO_{(l)}$ in intermediate atmosphere compositions (1.47% and 2.06%) has been attested by an exothermic peak in the DTA signal during cooling. The presence of chemical impurities such as Ca and Si may explain the appearance of the liquid phase $CrO_{(l)}$ at temperatures lower than that expected by the thermodynamic predictions. The amount of Cr volatilization depends of temperature and oxygen potential in the same way as does the $Cr_{(g)}$ equilibrium partial pressure of the considered reactions. Such conclusions will help to understand the behavior of Cr-doped UO_2 pellets during similar conditions of temperature and oxygen potential.

III.3.2. Solubilization of Cr_2O_3 in UO_2

The doped samples show a delay in densification compared to undoped UO_2 for each studied atmosphere. Bourgeois [12] observed this phenomenon during the sintering of UO_2 doped pellets which contain 0.31 mol% of Cr and using the following experimental conditions: 1%H_2O in hydrogen, heating rate of 2.5°C/min, use of spray-dried UO_2 powder. He explained this delay in densification by the development of a Cr_2O_3 film around the UO_2 particles. Delafoy [13] described the same effect, which increases with chromium content. So Cr_2O_3 fine particles dispersed in the UO_2 pellet probably inhibit the intergranular diffusion of ions during the first stage of sintering. Another mechanism can be considered, the surface diffusion of chromium cations on the UO_2 grains surface can also delay the intergranular diffusion.
As we previously noticed in the Section III.2.2 dedicated to the thermogravimetry experiments with doped pellets (for the 1.47% CO_2 atmosphere), it is interesting to compare the densification rate with the rate of mass loss. The maximum of the mass loss rate at 1200°C is close to that of the densification peak at 1157°C. These peaks could be due to the chromia solubilization in UO_2 accompanying the final step of the UO_{2+x} reduction. The mass loss rate difference when compared to the undoped UO_2 is probably due to the modification of the point defects nature and concentration in the doped UO_2 crystal structure. Similarly these defects contribute to the increase in the sintering rate. The slight differences between the peak temperatures of the DTG and densification rate curves probably come from the difference in the shape of the samples used in both experimental devices. The limit of solubility of chromia into UO_2 has been studied by several authors [4], [13], [14] and [15]. According to the Riglet-Martials data [15], it is possible to calculate the solubility for every condition of temperature and oxygen potential. The maximal fraction of dopant in solution into UO_2 during the heating may thus be evaluated. For example, at 1560°C and 1.47% CO_2, no more than 61% of the chromia introduced in the pellet can enter in solution in UO_2 in the case of 0.44 mol% Cr, and only 30% in the case of 0.9 mol% Cr. At 1640°C, these values move to 80% for 0.44 mol% Cr, and only 40% in the case of 0.9 mol% Cr. Thus, in reality, only a part of chromia enters in solution into the UO_2 crystal, the other part remaining in the form of Cr_2O_3 particles dispersed in the pellet. Since during the temperature increase, the porosity remains open during a given period, chromia is expected to dissociate according to the same process as that observed in the case of Cr_2O_3 powder. This certainly explains the similarity between the mass loss curves observed in Cr_2O_3 powder and Cr-doped UO_2 pellets. This is especially clear in the case of the 0.9 mol% Cr doped sample for which the mass loss rate continuously decreases after 1500°C up to 1700°C (Figure 8b). For a fixed oxygen potential, the higher the temperature, the higher the solubility. Considering the rate of mass loss and densification curves, it can be inferred that for kinetic reasons the solubilization process of Cr_2O_3 occurs majoritarily near 1200°C, then the "excess" chromia may be progressively incorporated in UO_2 as far as the solubility limit increases with temperature. However, the fraction of chromia which remains as Cr_2O_3 particles cannot be neglected with respect to their contribution to the volatilization process.

III.3.3. Sintering behavior of undoped and Cr-doped UO_2

For all the atmosphere compositions, a second acceleration of the densification occurs giving a maximum rate in the range 1500-1600°C, the higher the dopant amount, the higher the densification rate. Such an acceleration has to be compared to Chevrel'study [16] showing a similar effect during the sintering of overstoichiometric UO_2 containing numerous Willis type defects which are known to enhance the ions diffusion and thus accelerate the densification. In the present study, this phenomenon can be related to an increase in the Willis defects concentration as the result of chromium insertion at uranium sites of UO_2 crystals and distortion of the oxygen lattice around chromium ions [17]. Chromium ion in solution into UO_2 takes III + valency and disturbs a lot the chemical defects in the UO_2 matrix, producing mainly Willis type defects. For the 0.6% CO_2 atmosphere, in agreement with the thermodynamic diagram proposed by Toker *et al.* [5], the dissociation of $Cr_2O_{3(s)}$ in $Cr_{(s)}$ occurs at 1473°C (R2). Consequently, the presence of metallic chromium precipitates can pin the grain boundaries [12] explaining the low final density of the sample compared to the less reducing atmospheres. In the doped pellets the Cr volatilization process is expected to depend of the competition between the sintering and solubilization rates since the "excess" Cr_2O_3 particles will behave differently before and after the closure of the porosity. Before this point, the surface of the Cr_2O_3 particles is in contact with the surrounding atmosphere allowing $Cr_{(g)}$ transport in the gas phase, and beyond it, the volatilization of chromium necessitates bulk or/and grain boundary diffusion inside the UO_2 ceramic matrix.

III.3.4. Liquid phase

For the 0.9 mol% doped sample and the 1.47% and 2.06% CO_2 atmospheres, the densification rate curves exhibit a second peak close to 1660°C. Based on microstructure examinations, Bourgeois [12] explained such a phenomenon by the hypothesis of a liquid phase for the high Cr_2O_3 contents. TG-DTA results on chromia powder, for 1.47% CO_2 and 2.06% CO_2, validate this interpretation due to the exothermic peak associated to the crystallization of a liquid phase detected during the cooling period.

For the atmosphere 3.2% CO_2, and 0.9 mol% Cr doped sample, the dilatometric curve of the sintered doped pellet also shows a second acceleration of the densification, but at a higher temperature, near 1680°C. However in this case any exothermic DTA peak was observed during the cooling of the Cr_2O_3 powder. Open porosity can disappear when the ceramic density exceeds 95% *d*th, in the doped pellet the closure can began around 1680°C. At this temperature, the decomposition of $Cr_2O_{3(s)}$ in $Cr_{(g)}$ can take place with a chromium partial pressure close to 1×10^{-3} atm. Thus $Cr_{(g)}$ could be trapped in the closed porosity and react with $Cr_2O_{3(s)}$ to form liquid $CrO_{(l)}$ according to reaction R11. Moreover, considering the experiments done in the dilatometer furnace, the thermodynamic conditions may not be strictly the same outside and inside the sample just after the closure of the porosity. This may also contribute to the formation of the liquid phase.

The appearance of the $CrO_{(l)}$ liquid phase thus favors the sintering process and, as previously explained with the porosity closure effect, it may play indirectly a significant role in the chromium volatilization process.

III.3.5. Volatilization process from Cr-doped UO_2 pellets

The volatilization process from Cr-doped UO_2 pellets may be explained due to the comparison of the results obtained with the Cr_2O_3 powder. During the high temperature treatment from 1000 to 1700°C, the following phenomena have to be considered:

- A part of the added chromia solubilizes with a maximum rate around 1200°C, then the solubilization process may continue as far as the temperature increases, in relation to the corresponding solubility limit.
- At temperatures higher than 1480°C, and in all atmospheres, as far as the porosity remains open, the volatilization process consists of two contributions: one is the dissociation of excess chromia (not yet solubilized chromia) with a behavior similar to that of Cr_2O_3 powder (reaction R1); a second smaller contribution may come from $Cr_{(g)}$ volatilization from effectively Cr-doped UO_2 particles (soluble Cr) with a kinetic

behavior expected to be different from that of the chromia particles; indeed, in that case, the volatilization process needs chromium to diffuse into the UO_2 particles.

- After the porosity closure, which has been shown to be influenced by the appearance of the $CrO_{(l)}$ liquid phase, only one process should be considered: the volatilization needs the chromium to diffuse into the UO_2 matrix.

IV. Conclusions

The behavior of a chromium oxide powder at high temperature and under reducing atmospheres has been studied in details by combining DTA and thermogravimetry experiments. Experiments with a linear temperature increase up to 1700°C under various oxygen potentials where done to follow the chromia volatilization process. For all conditions, the results showed mass losses associated to endothermic signals. Based on thermodynamic considerations, the mass loss was principally attributed to the dissociation of Cr_2O_3 into gaseous metallic chromium and oxygen, and depending on the atmosphere composition, the formation of a liquid phase $CrO_{(l)}$ could be evidenced.

Dilatometry tests performed with undoped and Cr-doped UO_2 pellets allowed to determine the temperature domain where chromium is solubilized in UO_2, *i.e.* around 1100-1200°C, as well as the temperature at which the open porosity vanishes in the pellet. The presence of a liquid phase for the highest content of chromium was suggested from dilatometry measurements in good agreement with the DTA results with chromia powder.

The volatilization process during the sintering of doped UO_2 pellets has been shown to result from different phenomena: both decomposition of Cr_2O_3 particles (not solubilized in UO_2) and volatilization from Cr solubilized in UO_2 particles before the porosity closure, then Cr volatilization from the doped UO_2 ceramic matrix after the porosity closure. In the last case, both grain boundary and lattice diffusion processes have to be considered before volatilization, whereas only lattice diffusion is involved in the first case.

Concerning the application to the industrial nuclear fuel processing, further developments based on these conclusions could be achieved. In order to lower as far as possible the amount of chromium volatilization. Detailed kinetic study is in progress in order to quantify the kinetic rates of these various contributions and to obtain a predictive rate law able to find the optimal processing conditions as regards to both the chromia volatilization and the final density of the ceramic.

References

[1] C. Delafoy, P. Dewes, T. Miles, AREVA NP, Cr_2O_3-doped fuel development for BWRs, in: Proceedings of the 2007 International LWR Fuel Performance Meeting, San Francisco, California, September 30 - October 3, 2007.

[2] C. Delafoy, P. Dewes, AREVA NP, New UO_2 fuel development and qualification for LWRs applications, in: Proceedings of the 2006 TOPFUEL International Meeting on LWR Fuel Performance, Salamanca, Spain, October 22-26, 2006.

[3] L. Bourgeois, Ph. Dehaudt, C. Lemaignan, A. Hammou; J. Nucl. Mater., 297 (2001), pp. 313-326.

[4] A. Leeaners, L. de Tollenaere, C. Delafoy, S. Van den Berghe; J. Nucl. Mater., 317 (2003), pp. 62-68.

[5] N.Y. Toker, L.S. Darken, A. Muan; Met. Trans., 22B (1991), pp. 225-232.

[6] R.E. Johnson, A. Muan; J. Am. Ceram. Soc., 51 (1968), pp. 430-433.

[7] Y.I. OlShanskii, V.K. Shlepov, Systema Cr-Cr_2O_3, Mezhdunarodnaya kniga, vol. 91, 1953, pp. 561-564.

[8] P. Deines, R.H. Nafziger, G.C. Ulmer, E. Woermann; Bull. Earth Mineral Sci. Exp. Station, 88 (1975), pp. 1-129.

[9] O. Knacke, O. Kubaschewski, K. Hesselmann, Thermochemical properties of Inorganic substances, second ed., Springer, Berlin, 1991, pp. 2500.

[10] S. Degterov, A.D. Pelton; J. Phase Equilib., 17 (1996), pp. 476-494.

[11] T. Li, R.J. Brook, B. Derby; J. Eur. Ceram. Soc., 19 (1998), pp. 399-405.

[12] L. Bourgeois, Contribution à l'étude du rôle de dopants dans la densification et la croissance cristalline du dioxyde d'uranium, PhD Thesis, Science et Génie des Matériaux. Grenoble: INPG, 1992, pp. 137.
[13] C. Delafoy, Contribution à l'industrialisation de pastilles UO_2 à propriétés optimisées, Mémoire CNAM, Métallurgie, Lyon: CNAM, 2000, pp. 119.
[14] H. Keyklamp; J. Nucl. Mater., 247 (1997), pp. 103-107.
[15] C. Riglet-Martial, Proposition d'un modèle thermodynamique de solubilité du chrome dans le dioxide d'uranium, Personal Communication, 2006.
[16] H. Chevrel, Frittage à basse température du dioxyde d'uranium, en conditions de surstoechiométrie temporaire, PhD Thesis, Science des Matériaux, Limoges: Université de Limoges, 1990, pp. 116.
[17] M. Fraczkiewicz, Dopage au chrome du dioxyde d'uranium : modifications physiques induites, PhD Thesis, Ingénierie - Matériaux Mécanique Energétique Procédés Production, Grenoble: Institut Polytechnique de Grenoble, 2010, pp. 220.

Figures

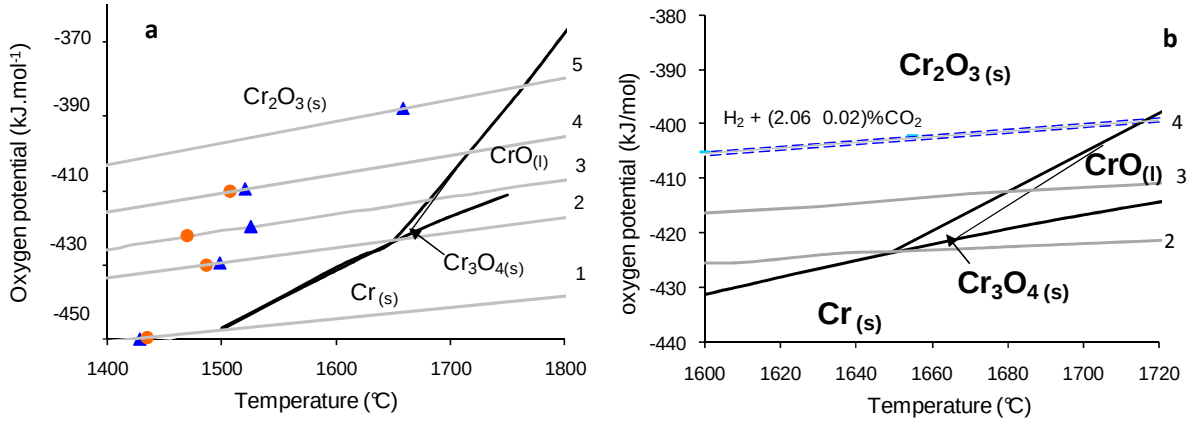

Figure 1: (a) Thermodynamic diagram for the Cr-O system according to Toker et al. [5] with the DTA signal start (●) and mass loss start (▲) for all atmospheres studied in this paper. H_2 + 0.6% CO_2 (1), H_2 + 1.11% CO_2 (2), H_2 + 1.47% CO_2 (3), H_2 + 2.06% CO_2 (4), and H_2 + 3.2% CO_2 (5). (b) Magnification of the diagram centered on the Cr_3O_4 domain and representation of the oxygen potential error (dashed line) for H_2 + 2.06% CO_2 atmosphere.

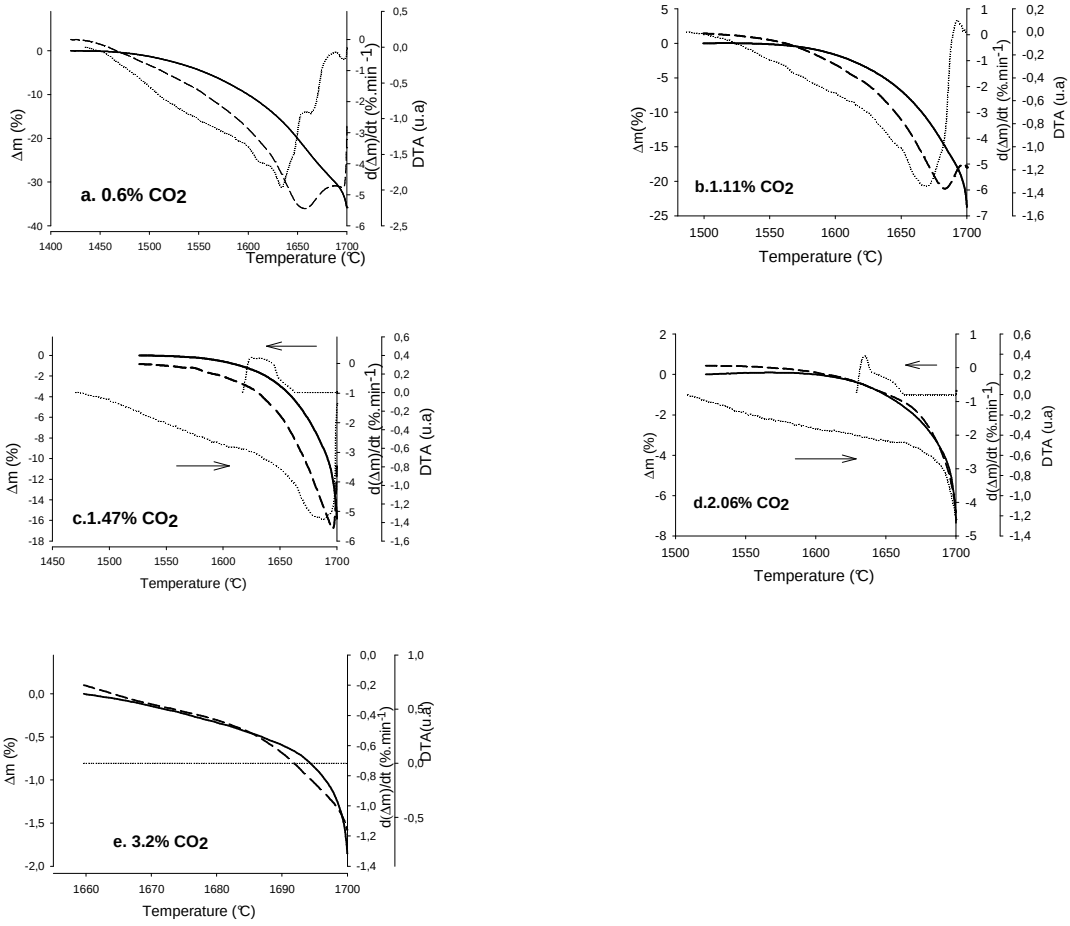

Figure 2: Mass loss Δm in% (–), rate of the mass loss d(Δm)/dt in% min^{-1} (––) and DTA signal (···) in arbitrary units for Cr_2O_3 powder under various H_2/CO_2 atmospheres with %CO_2 equal to 0.6 (a), 1.11 (b), 1.47 (c), 2.06 (d) and 3.2 (e).

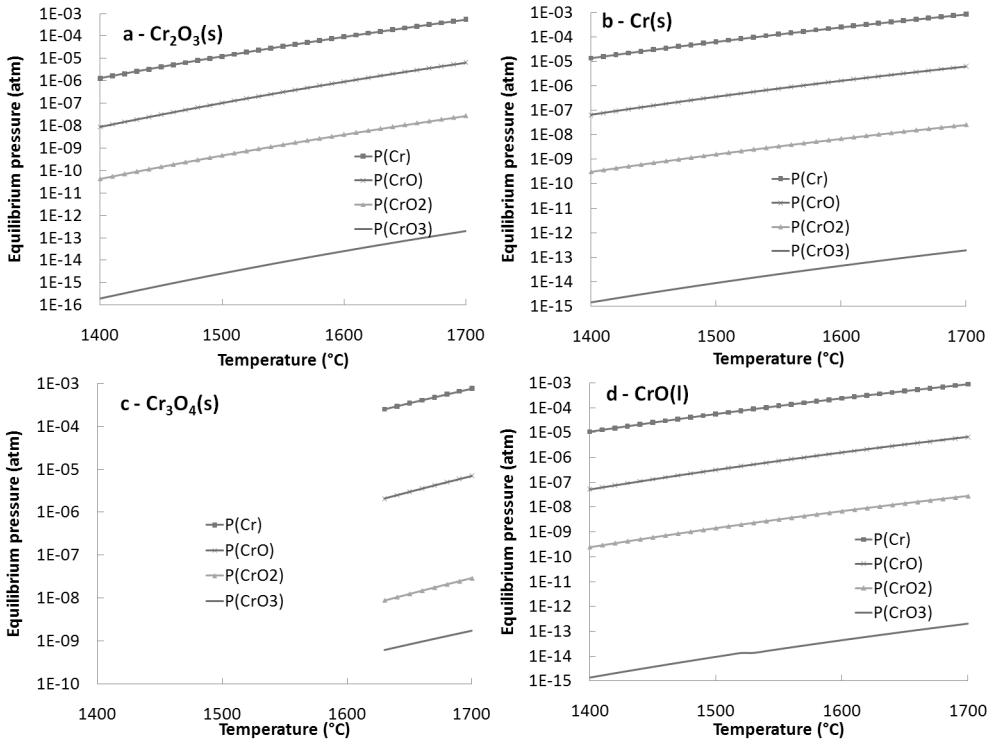

Figure 3: Calculated pressures of gaseous species $Cr_{(g)}$, $CrO_{(g)}$, $CrO_{2(g)}$ and $CrO_{3(g)}$ in equilibrium with solids or liquid $Cr_2O_{3(s)}$ (a), $Cr_{(s)}$ (b), $Cr_3O_{4(s)}$ (c) and $CrO_{(l)}$ (d) versus temperature for H_2 + 1.11% CO_2 atmosphere.

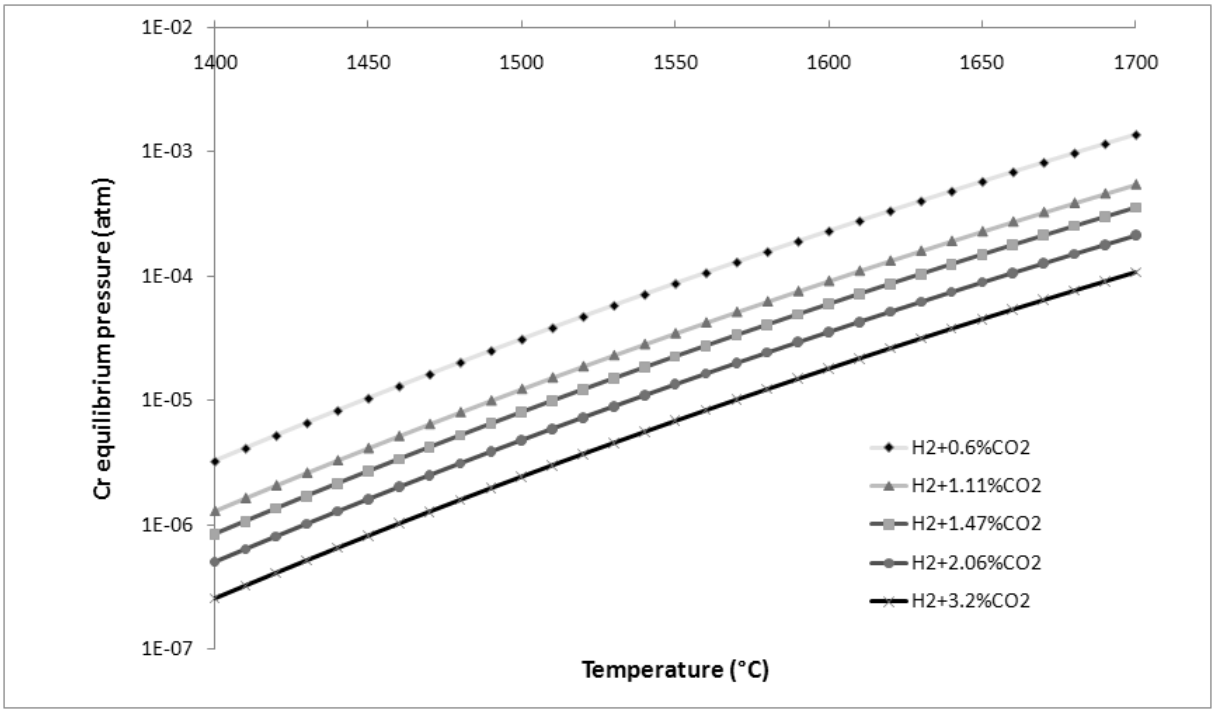

Figure 4: Calculated Cr(g) pressure in equilibrium with $Cr_2O_{3(s)}$ versus temperature for the various atmospheres used in this study.

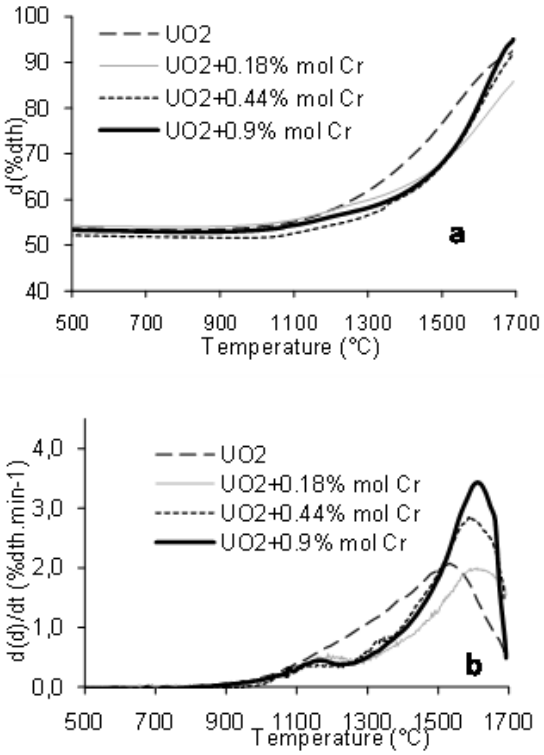

Figure 5: (a) Densification curves in %dth and (b) rate of densification in %dth min⁻¹ for UO_2, UO_2 + 0.18 mol% Cr, UO_2 + 0.44 mol% Cr and UO_2 + 0.9 mol% Cr in H_2 + 2.06% CO_2 atmosphere.

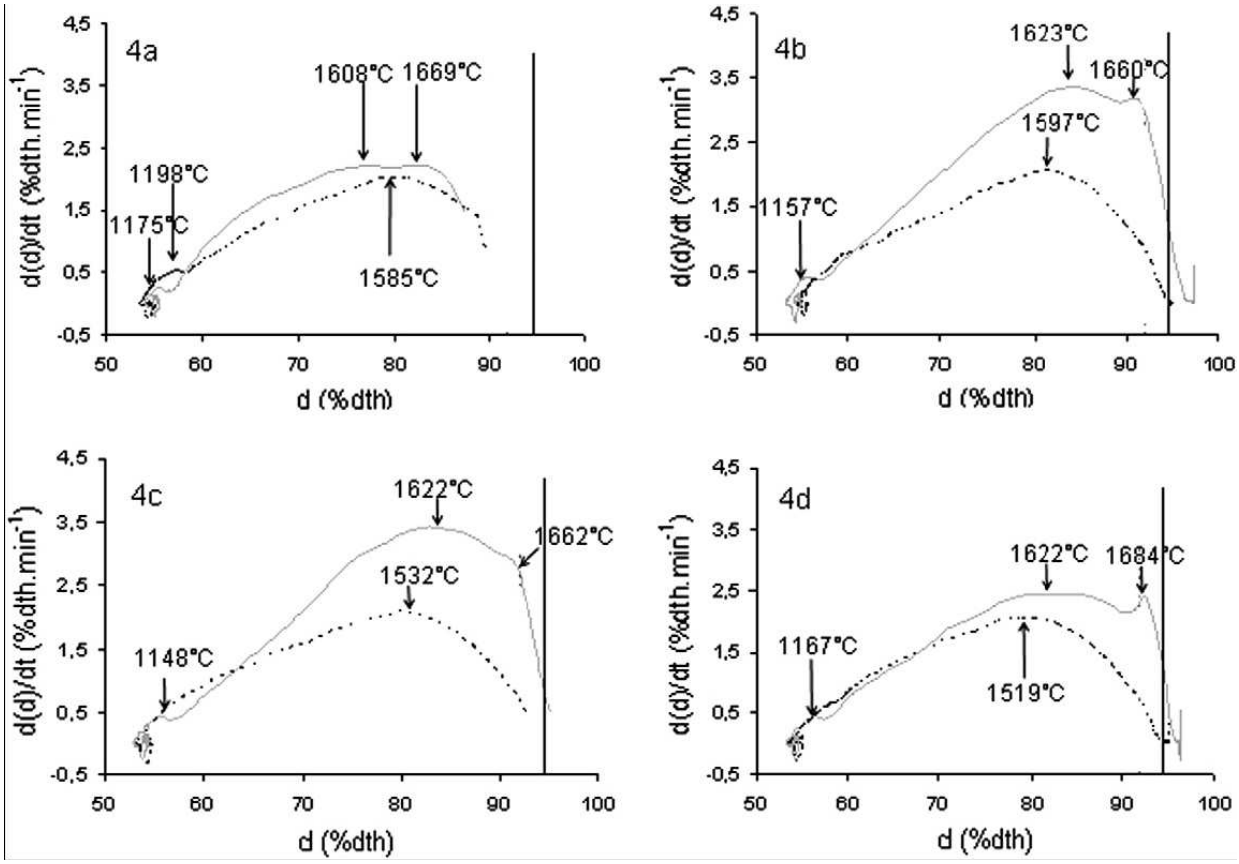

Figure 6: Rate of densification in %dth min⁻¹ for UO_2 (···) and UO_2 + 0.9 mol% Cr (–) under various H_2/CO_2 atmospheres with $\%CO_2$ equal to 0.6 (a), 1.47 (b), 2.06 (c) and 3.2 (d). The vertical lines correspond to 95% dth.

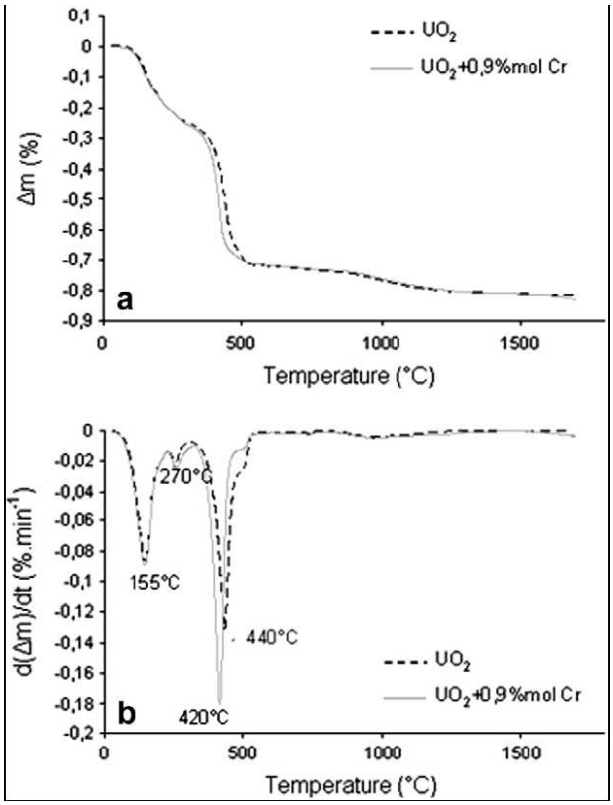

Figure 7: (a) Mass loss Δm in% and (b) rate of mass loss d(Δm)/dt in% min⁻¹ for UO2 (···) and UO2 + 0.9 mol% Cr (–) in H₂ +1.47% CO₂ atmosphere.

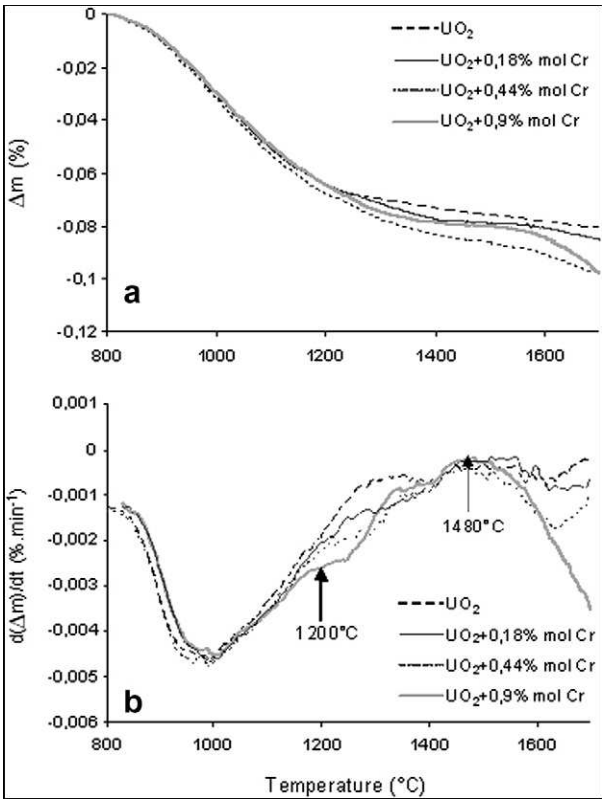

Figure 8: Mass loss Δm in% and (b) rate of mass loss d(Δm)/dt in% min⁻¹ for UO_2, UO_2 + 0.18 mol% Cr, UO_2 + 0.44 mol% Cr and UO_2 + 0.9 mol% Cr in H_2 + 1.47% CO_2 atmosphere.

Tables

Table 1: TG and DTA results for Cr_2O_3 powder.

% CO_2 in hydrogen	0.6%	1.11%	1.47%	2.06%	3.2%
TG: onset temperature (°C)	*1430*	*1499*	*1526*	*1521*	*1659*
dTG: peak temperature (°C)	*1663*	*1686*	*1697*	-	-
TG: Mass loss (%) at 1700°C	*35.9*	*23.8*	*15.9*	*7.4*	*1.9*
DTA: onset temperature (°C) (heating)	*1435*	*1487*	*1470*	*1508*	-
DTA: peak temperature (°C) (heating)	*1635*	*1671*	*1689*	-	-
DTA: onset temperature (°C) (cooling)	-	-	*1663*	*1662*	-
DTA: peak temperature (°C) (cooling)	-	-	*1624*	*1634*	-

Table 2: Standard (P = 1013 hPa) molar enthalpy variations and Gibbs energy variations of reactions at 1400 °C and 1700 °C [8,9] and theoretical mass loss for each reaction Ri.

Reactions	$\Delta_r H°$ (kJ.mol^{-1})		$\Delta_r G°$ (kJ.mol^{-1})		Theoretical mass loss (% of the reactive compound)
	1400°C	1700°C	1400°C	1700°C	
R1: $Cr_2O_{3(s)} \rightarrow 2Cr_{(g)} + 3/2\ O_{2(g)}$	*1891*	*1881*	*1028*	*879*	*100*
R2: $Cr_2O_{3(s)} \rightarrow 2Cr_{(s)} + 3/2\ O_{2(g)}$	*1129*	*1134*	*702*	*624*	*31*
R3: $Cr_{(s)} \rightarrow Cr_{(g)}$	*381*	*373*	*156*	*116*	*100*
R4: $Cr_2O_{3(s)} \rightarrow 2/3\ Cr_3O_{4(s)} + 1/6\ O_{2(g)}$	-	*191*	-	*73*	*3.5*
R5: $Cr_3O_{4(s)} \rightarrow 3Cr_{(g)} + 2\ O_{2(g)}$	-	*2535*	-	*1185*	*100*
R6: $Cr_3O_{4(s)} \rightarrow 3Cr_{(s)} + 2\ O_{2(g)}$	-	*1414*	-	*827*	*29.1*
R7: $Cr_3O_{4(s)} \rightarrow 3CrO_{(l)} + 1/2\ O_{2(g)}$	-	*583*	-	*207*	*7.3*
R8: $CrO_{(l)} \rightarrow Cr_{(g)} + 1/2\ O_{2(g)}$	*656*	*650*	*376*	*326*	*100*
R9: $Cr_2O_{3(s)} \rightarrow 2\ CrO_{(l)} + 1/2\ O_{2(g)}$	*580*	*579*	*267*	*211*	*10.5*
R10: $CrO_{(l)} \rightarrow CrO_{(g)}$	*444*	*437*	*233*	*196*	*100*
R11: $Cr_2O_{3(s)} + Cr_{(g)} \rightarrow 3CrO_{(l)}$	*-76*	*-71*	*-109*	*-115*	-

Table 3: Dilatometry results for undoped and Cr_2O_3-doped UO_2 pellets.

$\%CO_2$ in hydrogen	0.6%		1.47%		2.06%				3.2%	
mol% Cr	*0%*	*0.9%*	*0%*	*0.9%*	*0%*	*0.18%*	*0.44%*	*0.9%*	*0%*	*0.9%*
Onset T(°C)	*1198*	*1175*	-	*1157*	-	*1209*	*1148*	*1178*	-	*1167*
Peak T(°C)	*1585*	*1608* *1669*	*1597*	*1623* *1660*	*1532*	*1610*	*1593*	*1622* *1662*	*1519*	*1622* *1684*
Density (% *d*th) at 1700°C	*90*	*87*	*93*	*96*	*92*	*86*	*91*	*95*	*93*	*94*